Macromolecules
ARTICLE

*Macromolecules* **2009**, *42*, 6647–6655 **6647**
DOI: 10.1021/ma9001269

# Influence of Annealing on Microstructure and Mechanical Properties of Isotactic Polypropylene with β-Phase Nucleating Agent

**Hongwei Bai,[†] Yong Wang,*[,†] Zhijie Zhang,[‡] Liang Han,[†] Yanli Li,[†] Li Liu,[†] Zuowan Zhou,[†] and Yongfeng Men[‡]**

[†]*Key Laboratory of Advanced Technologies of Materials (Ministry of Education), School of Materials Science & Engineering, Southwest Jiaotong University, Erhuan Road, North I, No. 111, Chengdu, Sichuan 610031, P. R. China, and* [‡]*State Key Laboratory of Polymer Physics and Chemistry, Changchun Institute of Applied Chemistry, Chinese Academy of Sciences, Graduate School of Chinese Academy of Sciences, Renmin Street 5625, 130022 Changchun, P. R. China*

*Received January 20, 2009; Revised Manuscript Received July 16, 2009*

ABSTRACT: The microstructure and mechanical properties of β-nucleated iPP before and after being annealed at different temperatures (90−160 °C) have been analyzed. Annealing induced different degrees of variation in fracture toughness of β-nucleated iPP samples, namely, slight enhancement at relatively low annealing temperatures (< 110 °C) and great improvement at moderate temperatures (120−130 °C), whereas dramatic deterioration at relatively high temperatures ( > 140 °C) has been observed. The variation of fracture toughness of β-nucleated iPP is observed to be dependent on the content of β-NA. Experiments, including scanning electronic microscope (SEM), wide-angle X-ray diffraction (WAXD), differential scanning calorimetry (DSC), small-angle X-ray scattering (SAXS), and dynamic mechanical analysis (DMA), are performed to study the variations of microstructures as well as the toughening mechanism of the β-nucleated iPP after being annealed. The results indicate that the decreased number of chain segments in the amorphous region and the formation of microvoids, which is easily triggered by the secondary crystallization at 120−130 °C, are mainly responsible for the great improvement of toughness through promoting the lamellae to slip or elongate along the impact direction and inducing the intense plastic deformation during the fracture process.

## 1. Introduction

Isotactic polypropylene (iPP) is a polymorphic material with several crystal modifications including monoclinic α-phase, the trigonal β-phase, the orthorhombic γ-phase, and smectic mesophase (intermediate state between ordered and amorphous phase), all sharing the same 3-fold conformation but with different spatial arrangements of iPP chains in the crystal lattice.[1−28] The monoclinic α-phase, a thermodynamically stable phase and predominating under normal processing conditions, is characterized by the so-called "cross-hatched" lamellar morphology for radial α-spherulites with positive or mixed birefringence, which is first observed by Binsbergen and de Lange[1] and later on studied extensively by Lotz.[2] As for the orthorhombic γ-phase, it can be obtained when crystallization occurs at elevated pressure or the matrix exhibits low molecular weight as well as some defects in the main chain, for example, in random copolymers of polypropylene.[5−7] The β-phase is a thermodynamically metastable phase, and it is sporadically observed in commercial grades of iPP products at higher undercooling. Crystallization in the shear stress field,[8−11] in a temperature gradient,[12] or with active β-phase nucleating agent (β-NA)[11,13−25] encourages the numerous formations of β-iPP. β-iPP crystallizes in the spherulitic form, too, and two types of β-spherulites can form: the radial and the ringed spherulites, both with strong negative birefringence. It has been shown that hedrites (hexagonite) form in the early stage of the crystallization of β-iPP, which then grow further to ovalites and then to spherulites. Depending on the steric position of the hedrites and on the maturity of the supermolecular, different formations can be observed for the same sample.[26−28]

Because of the differences in the supermolecular structures, the different crystalline states of iPP exhibit different mechanical features. α-iPP shows excellent modulus and tensile strength but inferior fracture toughness because the presence of interlocking effect of the radial lamellae by the tangential crystallites makes the plastic deformation very difficult.[29−31] However, β-iPP without cross-hatching allows the initiation and propagation of plastic deformation more easily and then enhances the energy dissipating processing.[30−34] Especially, Karger-Kocsis proposed that the enhanced toughness of β-iPP can be attributed to a stress-induced transformation from less dense (β-phase) to more dense (α-phase) crystalline structure at the root of a growing crack.[28,35]

However, the fracture toughness does not increase monotonically with the increase of β-iPP content, which increases with β-NA content. It has been reported that there is a "critical" β-NA content (0.03−0.05 wt %) for iPP with the superior fracture toughness.[36,37] The microstructure is investigated to explain the reason why the sample exhibits the excellent toughness at the "critical" β-NA content. Small-angle X-ray scattering (SAXS) result indicates that the excellent toughness is resulted from a minimum of lateral dimensions of the crystallites and an optimum thickness of the amorphous interlayer with connecting chains between the β-lamellae.[37] Other investigation proves that the different mechanical behaviors of the critically nucleated and the supercritically nucleated β-iPP can be explained by the differences in supermolecular morphologies.[38] The former contains well-developed β-spherulites, while the latter shows bundlelike morphology without distinctly developed spherulites. And recently, researches from Varga and Menyhárd[39] show that

*Corresponding author: Tel +86-28-87602714, Fax +86-28-87600454, e-mail yongwang1976@163.com.



Published on Web 07/24/2009

the existence of "critical $\beta$-NA content" is related to the solubility and the dual nucleating ability of $\beta$-NA (*N,N′*-dicyclohexyl-2,6-naphthalenedicarboxamide). The enhanced fracture toughness of samples with "critical" nucleator content is attributed to the full dissolution of $\beta$-NA in iPP melt and the recrystallization from the melt in finely dispersed form, which induces a very uniform structure. However, in the "supercritically" nucleated samples, a part of introduced $\beta$-NA remains in the primary form, leading to the formation of a rougher and inhomogeneous supermolecular structure, which is disadvantageous for fracture toughness.

The microstructure and mechanical behaviors of $\beta$-iPP have also been comparatively researched recently through annealing process at the elevated temperature between glass transition temperature ($T_g$) and melting temperature ($T_m$).[40−43] It has been reported that annealing at temperatures higher than the upper limit of nucleation of $\beta$-phase results in an increase of the average lamellar thickness and narrowing of the distribution.[40,41] A pronounced "memory effect" has been observed during the annealing process.[42] Davies[43] studied the deformation and structural change in $\beta$-iPP by using synchrotron X-ray scattering coupled with in situ mechanical testing, and the results show that the ductility decreases with increasing annealing temperatures, different from the annealed α-iPP with enhanced fracture toughness.[44−46] However, compared to α-iPP with the interlocked structure, it seems more likely that $\beta$-iPP with the radial and/or the ringed spherulites as well as the thicker amorphous interlayer between interlamellae has more potential to be toughened by secondary crystallization occurring in the amorphous phase during annealing. With the improvement of the crystal induced by secondary crystallization, including the degree of crystallinity, molecular arrangement, and lamellae thickness, the fracture toughness in the bulk crystals increases because more fracture energy is needed to destroy this improved crystal structure.

Thus, in this study, our attention is paid to the variation of fracture toughness of $\beta$-iPP after being annealed. A highly effective $\beta$-NA aryl amides compound is introduced into iPP to achieve high level of $\beta$-iPP. 0.05 and 0.2 wt % $\beta$-NA are selected because the former content is proved to be the critical content, and the latter is the supercritical one for iPP.[22−24] All the nucleated iPP and neat iPP samples are annealed at different temperatures. The effect of annealing on the impact toughness of $\beta$-iPP is found to be tremendous. The possible fracture mechanisms of the annealed samples have been analyzed based on the investigation of microstructures changes during the annealing process.

## 2. Experimental Section

**2.1. Materials.** All the materials used in this study are commercially available. iPP (trade name F401) with a melt flow rate (MFR) of 2.5 g/10 min (230 °C/2.16 kg) was obtained from Langang Petrochemical Co, Ltd., Lanzhou, China. The $\beta$-NA arylamides compound (trade name TMB-5) with a melt temperature of 348.9 °C was provided by Fine Chemicals Department of Shanxi Provincial Institute of Chemical Industry, China. According to the simple analysis of the FTIR results of TMB-5 (chemical absorption positions at 3320, 2940, 2850, 1630, 1540, and 1330 $cm^{-1}$, not shown here), one can deduce that TMB-5 has a similar chemical structure compared to some aromatic amine $\beta$-phase NA, such as *N,N′*-dicyclohexyl-2,6-naphthalenedicarboxamide.[39]

**2.2. Sample Preparation.** To achieve a good dispersion of NA in iPP, a two-step process was employed to prepare the materials. Namely, a master batch of 5 wt % NA in iPP was first prepared through melt blending of TMB-5 and iPP, and then the master batch was melt blended with different contents of iPP to obtain the corresponding compositions (iPP with 0.05 wt % TMB-5 and 0.2 wt % TMB-5, shown as iPP/0.05TMB and iPP/0.2TMB, respectively). The melt blending of such samples was conducted on a twin-screw extruder (TSSJ-25, China) at a screw speed of 120 rpm and melt temperatures of 150−215 °C from hopper to die. After making droplets, the pellets were injection-molded, and the standard specimens for impact test were prepared using an injection-molding machine (K-TEC 40, Germany) at the melt temperatures of 190−215 °C from hopper to nozzle and a mold temperature of 25 °C.

The specimens were annealed for 12 h in a fan-assisted oven at different temperatures (90−160 °C). After being annealed, the specimens were cooled in the ambient air and then conditioned at 23 °C and 50% relative humidity for 48 h before testing. Here, the number after the notation of each annealed sample represents its corresponding annealing temperature. For example, iPP/0.05TMB-90 means that the sample of iPP/0.05TMB was annealed at 90 °C for 12 h.

**2.3. Mechanical Testing.** Notched Izod impact strength was measured using an impact tester (XC-22Z, China) according to ASTM D 256-04. For each sample, the average value reported was derived from at least five specimens. All the measurements were carried out at room temperature (23 °C). Tensile testing was conducted on a dumbbell-shaped specimen using an Instron 5567 tensile testing machine (USA) in accordance with ASTM D 638-03. A crosshead speed of 50 mm/min was used. Dynamic mechanical analysis (DMA) testing was carried out using a DMA Q800 analyzer. The single cantilever mode was selected, and the measurement was carried out on a rectangular cross-sectional bar of $40 \times 10 \times 4.2$ $mm^3$ (length × width × thickness) from −40 to 150 °C, at a heating rate of 3 °C/min and a frequency of 1 Hz.

**2.4. Scanning Electron Microscopy (SEM).** The impact-fractured surface and supermolecular structure of $\beta$-nucleated iPP were characterized by using a Fei Quanta 200 environmental scanning electron microscope (ESEM) with an accelerating voltage of 20 kV. For the impact-fractured surface, which was prepared by a notched Izod impact test at 23 °C, the observations were focused on the regions of crack propagation. For the supermolecular structure of iPP matrix, the injection-molded bar was first cryogenically fractured in the direction perpendicular to flow direction, and then the cryogenically fractured surface was etched for 18 h with an etchant containing 1.3 wt % potassium permanganate ($KMnO_4$), 32.9 wt % concentrated sulfuric acid ($H_2SO_4$), and 65.8 wt % concentrated phosphoric acid ($H_3PO_4$), according to the procedure proposed by Olley et al.[47] The core zone of the injection-molded bar was characterized because it is determinable in the whole sample. Furthermore, the cryofractured surface morphologies of unannealed and annealed samples prepared in liquid nitrogen were also investigated using SEM. Before SEM characterization, all the samples were sputter-coated with gold.

**2.5. Differential Scanning Calorimetry (DSC).** The melting behaviors of the samples were carried out on a Netzsch STA 449C Jupiter (Germany) in a nitrogen atmosphere. A sample of about 8 mg was heated from 30 to 200 °C at 10 °C/min. The fraction of $\beta$-phase ($f_\beta$) in the matrix can be calculated from the following equation:

$$f_\beta\,(\%) = \frac{X_{c\beta}\,(\%)}{X_{c\alpha}\,(\%) + X_{c\beta}\,(\%)} \times 100\% \quad (1)$$

where $X_{c\alpha}$ (%) and $X_{c\beta}$ (%) are the degrees of crystallinity for α-phase and $\beta$-phase, respectively.

The degree of crystallinity ($X_c$ (%)) for each sample was calculated by

$$X_c\,(\%) = \frac{\Delta H_m}{\Delta H_m^0} \times 100\% \quad (2)$$

where $\Delta H_m$ is the DSC measured value of fusion enthalpy, and

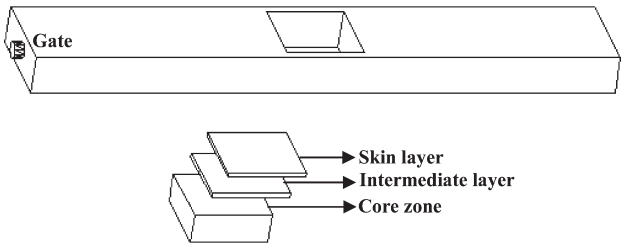


**Figure 1.** Schematic representation of sample cutting procedures from an injection-molded bar.

$\Delta H_m^0$ is the fusion enthalpy of the completely crystalline iPP. Here, the values of $\Delta H_m^0$ for α-iPP and $\beta$-iPP are selected as 177.0 and 168.5 J/g,[48] respectively.

**2.6. Wide-Angle X-ray Diffraction (WAXD).** The crystalline structures of $\beta$-iPP were investigated using a wide-angle X-ray diffraction (WAXD, Panalytical X'pert PRO diffractometer with Ni-filtered Cu Kα radiation at 40 kV and 40 mA). It has been reported that for the injection-molded bar the sample usually exhibits the multilayer structures due to the different cooling rates and the influence of shear stress on microstructure.[49,50] Thus, the injection-molded bar was separated as three different layers: the skin layer (0 mm), the intermediate layer (0.5 mm away from the skin layer), and the core zone (1 mm away from the skin layer). The schematic representation of the different zones cut from the injection-molded bar is shown in Figure 1. The angular range used was from 10° to 35° (2$\theta$). The $\beta$-phase fraction ($K_\beta$) was calculated from WAXD diffractograms according to the following relation:[51]

$$K_\beta = H_{300}^\beta/(H_{110}^\alpha+H_{040}^\alpha+H_{130}^\alpha+H_{300}^\beta) \quad (3)$$

where $H_{110}^\alpha$, $H_{040}^\alpha$, and $H_{130}^\alpha$ are the intensities of the (110), (040), and (130) reflections of the α-phase, respectively, and $H_{300}^\beta$ is the intensity of (300) reflection of $\beta$-phase.

**2.7. Small-Angle X-ray Scattering (SAXS).** SAXS experiments were performed using a NanoSTAR-U (BRUKER AXS INC.) with Cu Kα radiation (wavelength, $\lambda = 0.154$ nm). The generator was operated at 40 kV and 650 $\mu$A. Two-dimensional SAXS patterns were obtained using a HI-STAR detector. The sample-to-detector distance was $L_{SD} = 1074$ mm. The effective scattering vector $q$ ($q = (4\pi/\lambda)\sin\theta$, where 2$\theta$ is the scattering angle) at this distance ranges from 0.05 to 2 nm$^{-1}$.

## 3. Results and Discussion

**3.1. Determination of Annealing Effects on Mechanical Properties.** As shown in Figure 2, with the increase of annealing temperature ($T_a$), the impact strength of all samples increases slightly, then up to a maximum value, and then depresses with the further increase of $T_a$. However, the degree of variation in impact strength is different. For neat iPP, the impact strength changes slightly in the whole process. The similar results have been reported by others, and the reason is partly ascribed to the improvement of crystal perfection degree without the excessive reduction of the tie molecules number.[52,53] However, for nucleated iPP, one can observe a typical brittle−ductile−brittle (B−D−B) transition in impact strength with the increase of $T_a$. At relatively low $T_a$ (< 110 °C), the impact strength enhances slightly. At moderate $T_a$ (120−130 °C), a dramatically improved impact strength can be achieved, indicating an excellent toughening effect. For example, iPP/0.05TMB-130 shows the impact strength of 24.1 kJ/m$^2$, much higher than that of unannealed iPP/0.05TMB sample (8.8 kJ/m$^2$) and even 4 times higher than that of neat iPP annealed at the same $T_a$ (5.8 kJ/m$^2$). This means that through the

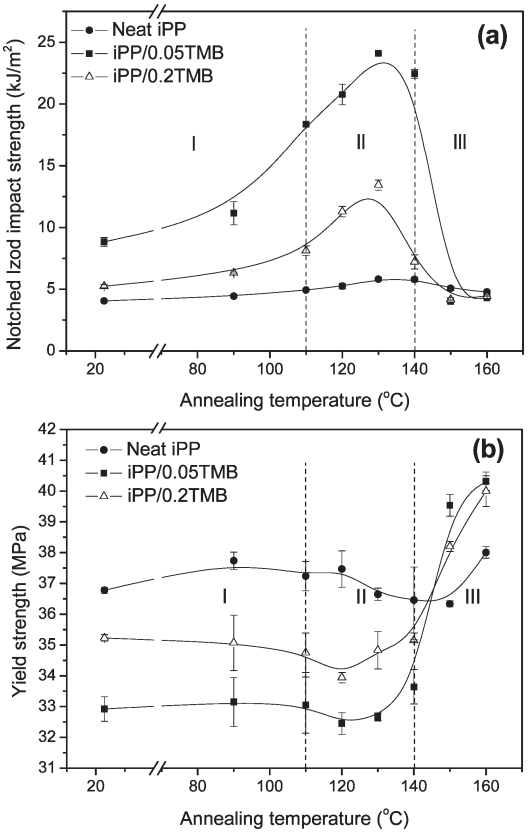


**Figure 2.** Notched Izod impact strength (a) and yield strength (b) of neat iPP and $\beta$-nucleated iPP samples after being annealed for 12 h at different temperatures.

combination of annealing process and the addition of $\beta$-NA the toughness of iPP is dramatically improved. Furthermore, one should notice that the annealing effect on impact strength is greatly dependent on the content of $\beta$-NA. iPP/0.05TMB exhibits a much higher impact strength compared to iPP/0.2TMB at wide range of $T_a$ (< 150 °C). However, further increasing $T_a$ (> 140 °C) depresses the impact strength significantly. The inferior impact strength of $\beta$-nucleated iPP is nearly comparable to neat iPP in this condition.

The yield strength of neat iPP and nucleated iPP as a function of $T_a$ is shown in Figure 2b. Similar to the variation of impact strength, the variation of yield strength with $T_a$ can be subclassified as different stages. For neat iPP, the yield strength increases slightly with $T_a$; except at 130−150 °C, the sample shows slight deterioration in average yield strength possibly due to the increased $\beta$-iPP content in the skin layer of the sample during the annealing process. It has been reported in our previous work that a few $\beta$-iPP are formed only in the skin layer of the iPP injection-molded bar;[54] during the annealing at 130−150 °C, the existing $\beta$-spherulites possibly invoke the further increasing of $\beta$-iPP. Annealing inducing the improvement of yield strength of neat iPP has been widely reported elsewhere, and the mechanisms are thought to be the improvement of crystal, the increase of lamella thickness, and the enhancement of the degree of crystallinity $X_c$ (%).[55] For unannealed nucleated iPP, it shows lower yield strength compared to neat iPP due to the formation of large amounts of $\beta$-iPP.[22−24] After being annealed, the yield strength decreases gradually with $T_a$ (< 120 °C), then down to a minimum value ($T_a$ = 120 °C), and then gradually increases with $T_a$ (> 120 °C). It is interesting to observe that when $T_a$ is higher than 150 °C,

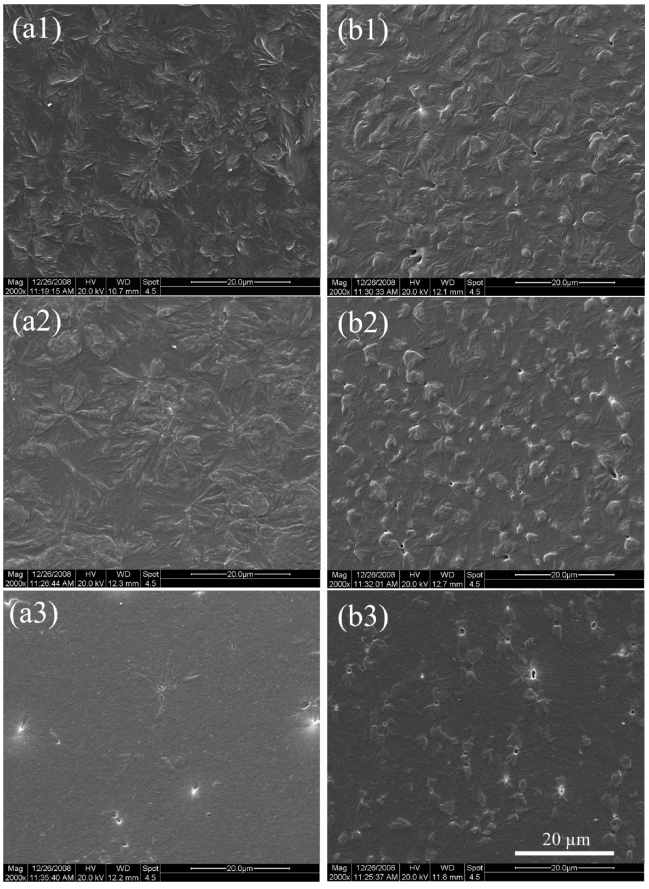


**Figure 3.** SEM images showing supermolecular structures of $\beta$-nucleated iPP injection-molded bar annealed at different temperatures for 12 h: (a1) iPP/0.05TMB-unannealed; (a2) iPP/0.05TMB-130; (a3) iPP/0.05TMB-150; (b1) iPP/0.2TMB-unannealed; (b2) iPP/0.2TMB-130; (b3) iPP/0.2TMB-150.

nucleated iPP even exhibits higher yield strength compared to neat iPP.

**3.2. Characterization of Microstructures before and after Being Annealed.** Figure 3 shows the supermolecular structures of $\beta$-iPP before and after being annealed, which were performed through combining of chemical etching and SEM. As expected, iPP/0.05TMB (the critically nucleated iPP) exhibits the well-developed spherulitic structures of $\beta$-iPP, while iPP/0.2TMB (the supercritically nucleated iPP) presents typically bundlelike morphology without distinctly developed spherulites. This can be explained by the different dissolution conditions of $\beta$-NA in critically and supercritically nucleated iPP.[39] In the former one, $\beta$-NA seems to be totally dissolved in iPP melt and recrystallize from the melt in finely dispersed form, which induces well-developed spherulites. In the latter one, most of $\beta$-NA, which cannot dissolve in iPP melt, separates from the melt, remains in the primary form, and distributes in the interlamellae and/or interface of $\beta$-iPP spherulites. This prevents the development of $\beta$-iPP spherulites and leads to the formation of a rougher and inhomogeneous supermolecular structure, for example, the bundlelike morphology. The difference in supermolecular structure has been proved to be the main reason for the different mechanical properties of these two materials.[37] It is important to recognize that, whether for iPP/0.05TMB-130 or for iPP/0.2TMB-130, the supermolecular structure almost remains unchanged after being annealed. This illustrates that the influence of annealing on supermolecular structure at $T_a$ of 130 °C is inconspicuous, and the supermolecular structure is mainly controlled by the content of $\beta$-NA. Similar results have been reported by Zia et al.[56] They found that annealing only permits a precise adjustment of the size and the thermodynamic stability of the iPP crystals, without affecting the external habit of the crystals and their organization in higher order structures. Thus, it can be said that, at moderate temperature ($T_a = 130$ °C), the microstructures of $\beta$-iPP may be refined during annealing process, although higher order structures remain unchanged. This will be further discussed in the following section by DSC and WAXD measurements. However, for iPP/0.05TMB-150 and iPP/0.2TMB-150, fewer $\beta$-iPP structures are observed. This can be ascribed to the partial melting and recrystallization of $\beta$-iPP at high $T_a$ (higher than the melting temperature ($T_a$) of $\beta$-iPP). Obviously, the deteriorated impact strength of $\beta$-nucleated iPP obtained at high $T_a$ is due to the dramatic decrease of $\beta$-iPP in the sample proved by SEM.

Since SEM images do not reveal the changes of fine microstructures, the variations of crystalline structures of $\beta$-iPP before and after being annealed were investigated by DSC and WAXD. As shown in Figure 4, after being annealed, annealed iPP shows a shoulder peak in the thermogram (premelting endothermic peak) before the main fusion peak of α-iPP, and the onset temperature of the shoulder peak increases gradually with the increase of $T_a$ (shown by the arrow), indicating that annealing induces a microstructural change which is dominated by the applied $T_a$. These observations are in agreement with the results reported in the literature, and the endothermic shoulder is attributed to the fusion of newly formed α-phase during the annealing, such as newly thin and imperfect lamella.[57,58] When $T_a$ is up to 160 °C, a significant increase of $T_m$ is observed for annealed iPP, indicating the apparent increase of lamella thickness.[59,60]

For $\beta$-nucleated iPP, there are similar results at all $T_a$ (Figure 4b,c). Two predominated fusion peaks are observed at approximate 148−155 and 168−175 °C (shown as $\beta$ and α, respectively), indicating the fusion of $\beta$-iPP and α-iPP.[20,61,62] The endothermic peak of α-iPP is ascribed to the phenomenon that, during the heating process of DSC measurement, the unstable $\beta$-iPP tends to melt first and recrystallize as α-iPP with more stable crystalline structure, which further melts at relative high temperature. After being annealed at high $T_a$ (> 140 °C), the main fusion peak of $\beta$-iPP disappears and a more intense fusion peak of α-iPP appears, suggesting the transition from $\beta$-iPP to α-iPP. Furthermore, one should notice that after being annealed at 150 and 160 °C both iPP/0.05TMB and iPP/0.2TMB show much higher $T_m$ (172 and 176 °C for $T_a$ of 150 and 160 °C, respectively) compared to iPP (about 167 and 173 °C) annealed at the same temperatures. This means that, through the transition of $\beta$-iPP to α-iPP induced by annealing at high $T_a$, the crystalline structures of α-iPP in iPP/0.05TMB and iPP/0.2TMB samples are more stable than that in neat iPP samples obtained in the same $T_a$. This is attributed to the fusion and recrystallization of $\beta$-iPP inducing more stable α-iPP formation with bigger thickness and less defects during the annealing process. As a consequence, higher yield strength is achieved for iPP/0.05TMB and iPP/0.2TMB samples after being annealed at high $T_a$.

Figure 5 shows the variation of $X_c$ (%) of iPP/0.05TMB and iPP/0.2TMB samples as the function of $T_a$. With increasing $T_a$ from 90 to 120 °C, a significant enhancement of $X_{c\beta}$ (%) (the degree of crystallinity of $\beta$-iPP) is observed, while invariant for $X_{c\alpha}$ (%). This indicates that the annealing at $T_a = 90-120$ °C induces the augment of $\beta$-iPP content. The higher the $T_a$ is, the more apparent the increase of $\beta$-iPP

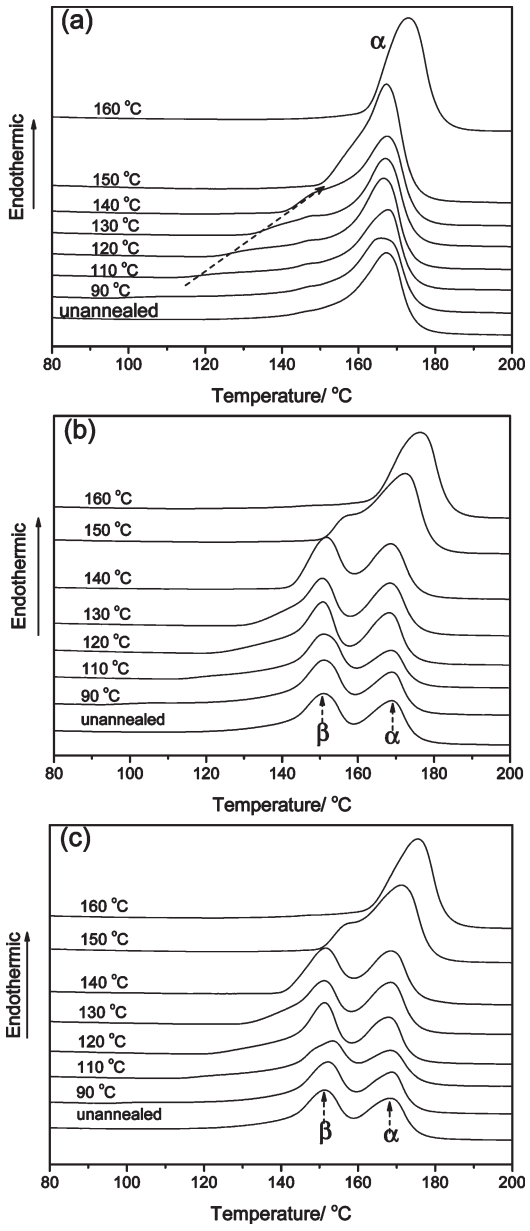


**Figure 4.** DSC heating curves of neat iPP and $\beta$-nucleated iPP samples after being annealed at different temperatures for 12 h: (a) neat iPP, (b) iPP/0.05TMB, and (c) iPP/0.2TMB. Note that the arrows indicate the progressing tendency of the onset temperature of premelting endothermic peaks.

content. This may be related to the transition of mesophase to $\beta$-iPP (in the front of growth plane of $\beta$-crystal) during the annealing process. However, with further increasing $T_a$, $X_{c\beta}$ (%) becomes deteriorated, whereas $X_{c\alpha}$ (%) increases gradually. The fraction of $\beta$-iPP ($f_\beta$ (%)) in the matrix also shows a great dependence on $T_a$. $f_\beta$ (%) increases with $T_a$, then up to the maximum value at about 110−120 °C, and then decreases with further increasing $T_a$. Obviously, annealing at 110−120 °C is in favor of the further increase of $\beta$-iPP in the $\beta$-nucleated iPP possibly due to the temperature is most favorable for the formation of $\beta$-iPP.[42,63] The decrease of $\beta$-iPP at high $T_a$ is due to the transition of $\beta$-iPP to more stable α-iPP proved by previous SEM results. Importantly, both iPP/0.05TMB-130 and iPP/0.2TMB-130 show the nearly invariant $X_{c\beta}$ (%) but increased $X_{c\alpha}$ (%) compared to the correspondingly unannealed samples, which suggests that the largely improved impact strength at $T_a$ of 130 °C

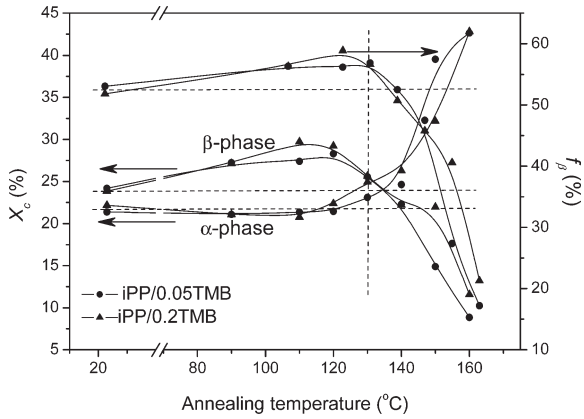


**Figure 5.** Variations of the degree of crystallinity ($X_c$ (%)) and the fraction of $\beta$-phase ($f_\beta$ (%)) in $\beta$-nucleated iPP with the annealing temperatures. Data were calculated from DSC measurements.

**Table 1. Distribution of $\beta$-Phase in the Different Zones of $\beta$-Nucleated iPP Injection-Molded Bar after Annealing at Different Temperatures[a]**

| | $K_\beta$ | | | $H^\beta_{300}$ (counts) | | |
|---|---|---|---|---|---|---|
| samples | skin layer | intermediate layer | core zone | skin layer | intermediate layer | core zone |
| iPP/0.05TMB-unannealed | 0.273 | 0.853 | 0.840 | 21 300 | 41 351 | 42 524 |
| iPP/0.05TMB-110 | 0.234 | 0.853 | 0.856 | 23 820 | 44 516 | 54 561 |
| iPP/0.05TMB-130 | 0.209 | 0.820 | 0.818 | 22 693 | 42 200 | 50 980 |
| iPP/0.05TMB-150 | 0.038 | 0.253 | 0.271 | 3 767 | 8 452 | 10 559 |
| iPP/0.2TMB-unannealed | 0.289 | 0.836 | 0.810 | 25 931 | 62 435 | 59 446 |
| iPP/0.2TMB-110 | 0.254 | 0.831 | 0.818 | 25 784 | 59 327 | 67 132 |
| iPP/0.2TMB-130 | 0.234 | 0.813 | 0.814 | 25 765 | 60 960 | 70 230 |
| iPP/0.2TMB-150 | 0.040 | 0.300 | 0.280 | 4 436 | 13 679 | 14 218 |

[a] $K_\beta$: the relative content of $\beta$-phase obtained by WAXD; $H^\beta_{300}$: the intensity of the strongest reflection peak of $\beta$-phase.

is not solely determined by the variations of crystalline structures.

The fine crystalline structures were further determined through WAXD measurement. To accurately describe the variation of $\beta$-iPP, the injection-molded bar was subclassified as three different layers, such as the skin layer, the intermediate layer, and the core zone. The details about $\beta$-iPP in different layers are shown in Table 1, and the typical WAXD profiles of samples cut from the core zone are shown in Figure 6. For unannealed sample, both iPP/0.05TMB and iPP/0.2TMB show the hierarchy crystalline structures in injection-molded bars. The contents of $\beta$-iPP in the intermediate layer and in the core zone are much higher than that in the skin layer. This can be ascribed to the relative high cooling rate presented in the skin layer, preventing the nucleation effect of $\beta$-NA.[49] After being annealed, the relative fraction of $\beta$-iPP decreases with increasing $T_a$; especially at $T_a = 150$ °C, the diffractions of $\beta$-iPP weaken dramatically, whereas more intensified diffractions are observed for α-iPP, indicating the transition from $\beta$-iPP to α-iPP during the annealing process. It is important to note that, for high $\beta$-iPP content sample, it is very difficult in fitting WAXD patterns due to the significantly lower intensities of α-iPP diffractions. Therefore, the intensities of $\beta$-iPP diffractions were collected to represent the relative magnitude of $\beta$-iPP content, and the credible degree of crystallinity of each phase (α-phase and $\beta$-phase) is not offered here.

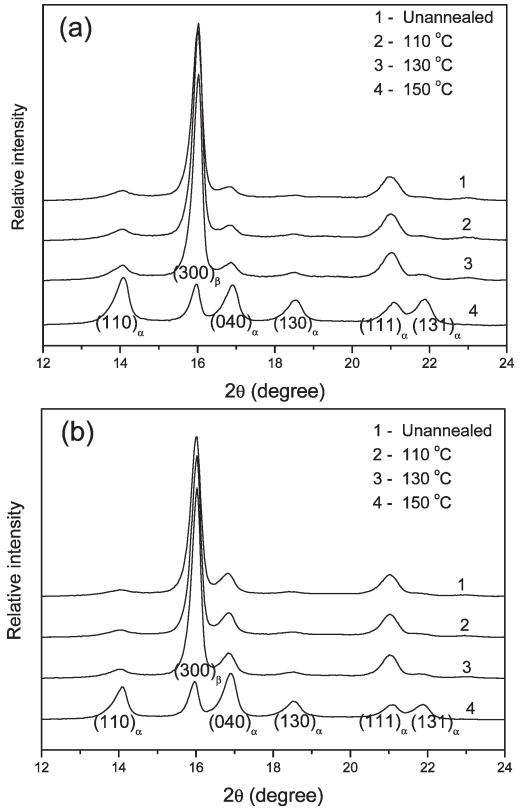


**Figure 6.** WAXD patterns of $\beta$-nucleated iPP samples after being annealed at different temperatures for 12 h: (a) iPP/0.05TMB and (b) iPP/0.2TMB. Samples were cut from the core zones of injection-molded bars.

Similar variation trends for nucleated iPP before and after being annealed are reported in Table 1.

Obviously, the observed transition of $\beta$-iPP to $\alpha$-iPP proved by SEM, DSC, and WAXD measurements can adequately explain the great deterioration of impact strength and the improvement of yield strength at high $T_a$ (> 140 °C). The variations of mechanical properties at low $T_a$ (< 110 °C) are ascribed to be the increase of $\beta$-iPP content during the annealing process. However, at $T_a$ of 120−130 °C, the slight increase of $\beta$-iPP is not enough to trigger such dramatic improvement of impact strength, and further explanation is needed.

**3.3. Further Investigation on the Toughening Mechanism of $\beta$-iPP Annealed at Moderate Temperatures.** To clearly understand the mechanism why the $\beta$-nucleated iPP samples exhibit the great improvement in impact strength after being annealed at 120−130 °C, the typical impact fractured surfaces of iPP/0.05TMB before and after being annealed at 130 °C were characterized, and the results are shown in Figure 7. For unannealed iPP/0.05TMB sample, relative smooth surface morphology without visible plastic deformation is observed, indicating the typical feature of brittle fracture mode. This observation is consistent with lower impact strength. For iPP/0.05TMB-130 sample, the surface morphology exhibits the ductile features with the formation of fibrillar structure as well as microvoids, suggesting more energy dissipating during impact fracture.[64−68] Importantly, one should notice that the fibrillar structure is always observed between or around microvoids, indicating that the fibrillar structure may be related to the intense plastic deformation of amorphous between microvoids.

In order to understand whether the cavities form in the $\beta$-nucleated iPP samples or not, unannealed and annealed

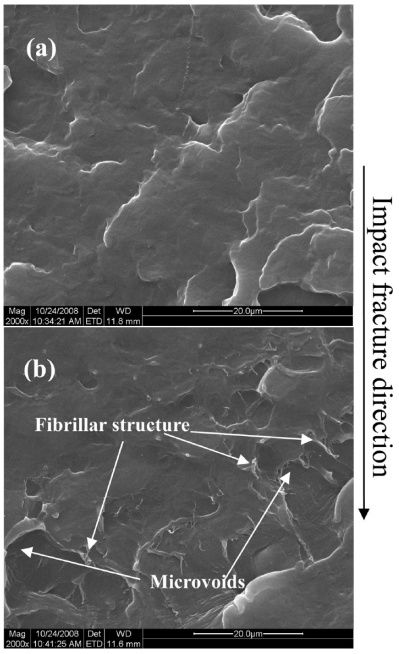


**Figure 7.** SEM images showing the typical impact-fractured surface morphologies of unannealed and annealed $\beta$-nucleated iPP: (a1) iPP/0.05TMB-unannealed; (a2) iPP/0.05TMB-130.

PP/0.05TMB-130 samples were investigated using SAXS, and the results are shown in Figure 8. For the unannealed sample, only X-ray scattering from crystalline structure of iPP is visible. After being annealed, the intensity of scattering seems to decrease slightly. As is well-known, the SAXS scattering intensities are dependent on the number and volume of scattering objects. The decreased scattering intensities are contradictory to the changes of crystalline structures as proved by SEM, DSC, and WAXD measurements. According to the methodology proposed by Glatter,[69] the plots of $Iq^2$ vs $q$ are shown in Figure 8d. One can see that the position of maximum scattering intensity keeps invariant before and after being annealed, implying that the crystalline lamellar long spacing is not changed (calculated as 24.14 nm). Although SAXS has been proved to be very efficient in proving the presence of cavities,[70] our SAXS results show that there are no cavities formation during the annealing process.

Thus, the cryofractured surface morphologies of unannealed and annealed PP/0.05TMB-130 samples were investigated using SEM, too. As shown in Figure 9, the unannealed sample exhibits homogeneous surface morphology whereas different surface morphology with very small black holes is observed for annealed sample, which really indicates the presence of microvoids formed during the annealing processing.

The variation of microstructure and the toughening effect are further investigated using DMA, and the results are shown in Figure 10 and Table 2. The mechanical loss factor (tan $\delta$) curve exhibits two maxima. The maximum at low temperature (12−17 °C) is related to $\beta$-relaxation, accounting for the glass transition of the unrestricted amorphous iPP, while the peak at the higher temperature is related to $\alpha_c$-relaxation, accounting for the relaxation of restricted iPP amorphous chains in the crystalline phase (defects), also known as rigid amorphous molecules.[71,72] Herein, glass transition temperatures ($T_g$) were obtained by the maximum of the loss factor (tan $\delta_{max}$) or $\beta$-relaxation peak. The magnitude of the $\beta$-relaxation ($I_R$) was determined by the

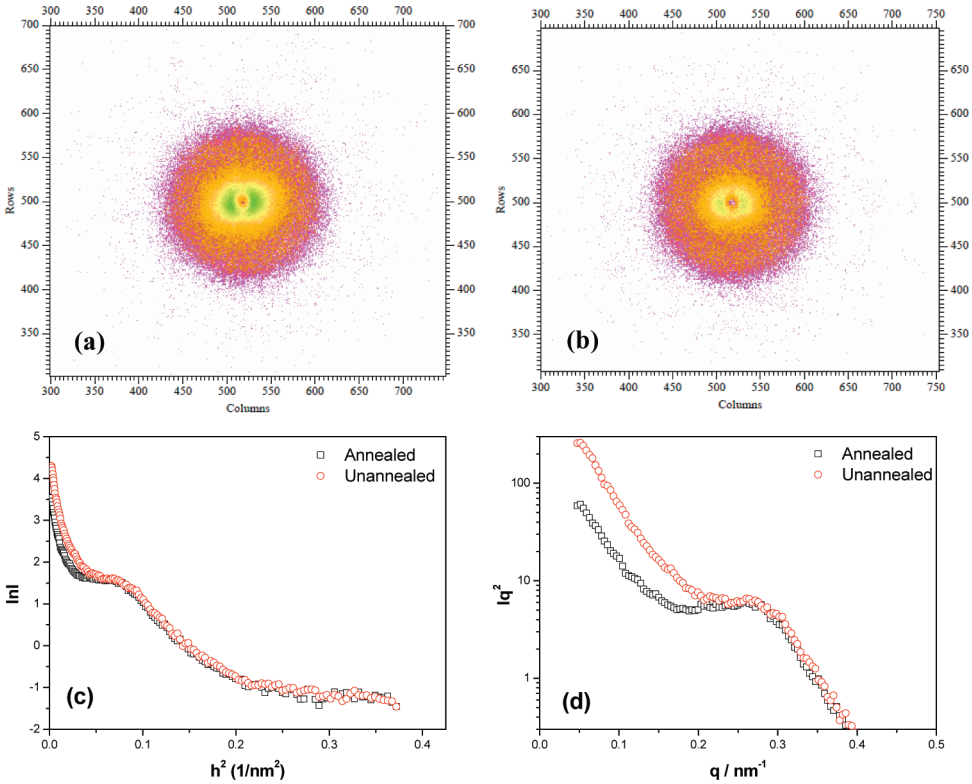


**Figure 8.** SAXS patterns for (a) unannealed iPP/0.05TMB and (b) annealed iPP/0.05TMB-130 samples. (c) Natural logarithm of SAXS intensities (ln $I$) plotted as a function of a scattering vector $h$ and (d) plots of $Iq^2$ vs $q$.

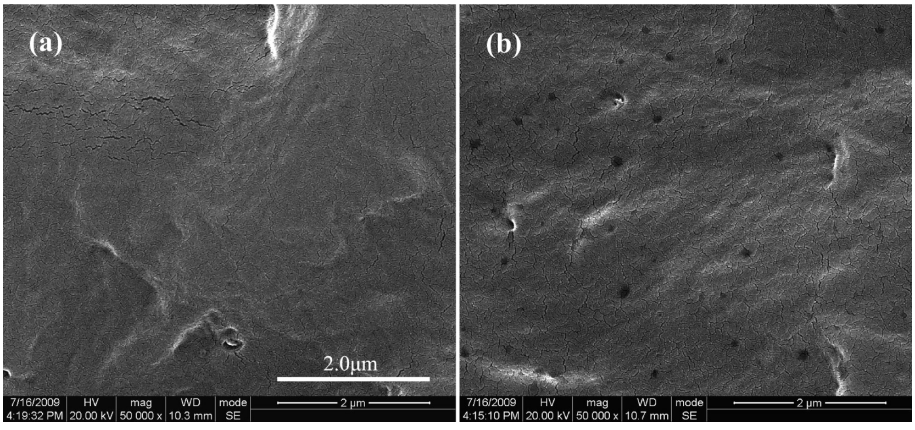


**Figure 9.** SEM images showing the cryrofractured surface morphologies of unannealed and annealed $\beta$-nucleated iPP: (a1) iPP/0.05TMB-unannealed; (a2) iPP/0.05TMB-130.

area under the $\beta$-relaxation peak. Compared with unannealed $\beta$-iPP (including iPP/0.05TMB and iPP/0.2TMB), $T_g$ decreases significantly by annealing at 130 °C, indicating that annealing promotes the motion ability of iPP amorphous chains possibly due to a decrease in the concentration of the chain segments in the amorphous phase.[46,73] In addition, it can be seen from Figure 9 that annealing at 130 °C promotes a significant increased temperature corresponding to $\alpha_c$-relaxation peak, which can be explained by the increase of rigid amorphous molecules,[57] resulting from the transition of mesophase to $\beta$-phase occurring near the surface of primarily formed $\beta$-lamella and the further perfection of primary $\beta$-lamella. Especially, some defects are introduced into the newly formed $\beta$-lamella during the second crystallization process, which results in more energy requirement for $\alpha_c$-relaxation to occur.[74]

DMA has also been proved to be a useful tool in estimating the fracture toughness of polymer and its blends.[75−77] The increase in tan $\delta_{max}$ and $I_R$ is representative of respectively the maximum and total energy dissipated because of viscoelastic relaxation of iPP component. As expected, annealing at 130 °C induces a significant increase of tan $\delta_{max}$ and $I_R$, indicative of the improved damping capacity. Generally, the impact toughness can be reflected by the magnitude of the $\beta$-relaxation ($I_R$).[75,76] The results also confirm that annealing at moderate temperature induces the improvement of impact toughness and damping capacity simultaneously.

Thus, it is believed that the decreased number of chain segments in the amorphous region between interlamellae is mainly responsible for the great improved fracture toughness after being annealed at 120−130 °C. For $\beta$-iPP, the motion of

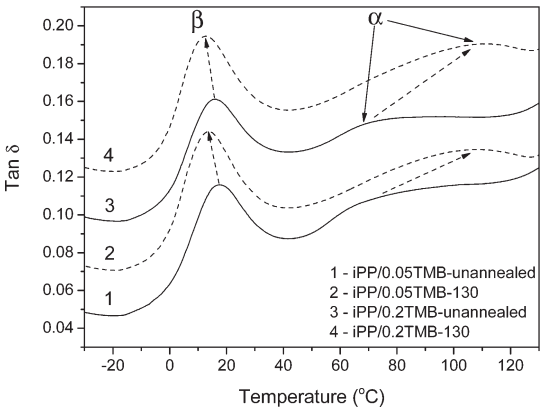


**Figure 10.** Comparison of mechanical loss factor (tan $\delta$) between unannealed and annealed $\beta$-nucleated iPP.

**Table 2. $\beta$-Relaxation Parameters Obtained from DMA Testing for Unannealed and Annealed $\beta$-Nucleated iPP[a]**

| samples | $T_g$ (°C) | tan $\delta_{max}$ | $I_R$ (arb units) |
|---|---|---|---|
| iPP/0.05TMB-unannealed | 17.48 | 0.1160 | 1.09 |
| iPP/0.05TMB-130 | 13.35 | 0.1340 | 1.29 |
| iPP/0.2TMB-unannealed | 15.53 | 0.1212 | 1.07 |
| iPP/0.2TMB-130 | 12.34 | 0.1245 | 1.29 |

[a] tan $\delta_{max}$: the maximum of mechanical loss factor; $T_g$: glass transition temperature; $I_R$: the magnitude of the $\beta$-relaxation.

the chain segments in the amorphous region of $\beta$-iPP is more available than that in α-iPP with the interlocked structure. During the annealing process, some chain segments further crystallize and enter into the lamellae, resulting in the decrease of chain segments amount in this region. Normally, the chain segments between interlamellae play an important role of transferring the load through the whole sample, and the decreased numbers of chain segments usually result in the interlamellae fracture. And as a consequence, the sample becomes more brittle. However, the decreased numbers of chain segments in the amorphous region also produce larger stress concentrations and promote yielding at lower stress levels.[78] In other words, the intralamellae structure becomes looser for each other and more available to slip or elongate along the impact direction, leading to large plastic deformation with more fracture energy absorption on the one hand. Thus, we believe that in this work the latter effect dominates the fracture of the annealed samples. On the other hand, the decreased number of chain segments between interlamellae possibly enlarges the differences between crystalline region and amorphous region, leading to the nucleation of microvoids in the vicinity of lamellae during the impact process, which provides stress concentration centers. Furthermore, the viscoelastic plastic processes are associated with the growth of microvoids and the deformation of ligaments bridging the microvoids. The ligaments or islands of material between the microvoids must fracture before the final separation occurs.[64] Besides the microvoids formed during the annealing processing, the decreased number of chain segments between interlamellae most likely is favorable to the nucleation and growth of new microvoids during the fracture process, changing the viscoelastic plastic processes and leading to the improvement of fracture toughness. Further work needs to be done to prove the formation of cavities in the annealed $\beta$-iPP sample is more available.

## 4. Conclusions

In summary, the mechanical properties and microstructures of neat iPP and $\beta$-nucleated iPP samples obtained before and after being annealed at different temperatures (90−160 °C) have been comparatively investigated. At low $T_a$ (< 110 °C), the impact strength of $\beta$-nucleated iPP increases slightly whereas yield strength decreases due to the increase of $\beta$-iPP content which is realized from the transformation of mesophase to $\beta$-phase during the annealing process. At moderate $T_a$ (120−130 °C), although the temperature is proved to be the best one for nucleation and growth of $\beta$-iPP, the increased amount of $\beta$-iPP is relatively small. Because of the second crystallization from the amorphous region, the number of chain segments in this region decreases and some microvoids form, making the lamellae structures looser and more available to slip and/or elongate along the impact direction. This is believed to be responsible for the significantly improved fracture toughness. At high $T_a$ (> 140 °C), most of $\beta$-iPP are replaced by α-iPP due to the melt-recrystallization process and more stable α-lamellae with bigger thickness are observed. As a consequence, a great deterioration in impact toughness and an apparent improvement in yield strength are reported. This work proves that, for $\beta$-nucleated iPP, annealing at appropriate temperature is an efficient way to further improve the fracture toughness of iPP without apparently impairing the yield strength.

**Acknowledgment.** The authors express their sincere thanks to Program for New Century Excellent Talents in University (NCET-08-0823) and Sichuan Youthful Science and Technology Foundation (07ZQ026-003) (P.R. China) for supporting this work.

## References and Notes

(1) Binsbergen, F. L.; de Lange, B. G. M. *Polymer* **1968**, *9*, 23–40.
(2) Lotz, B.; Wittmann, J. C.; Lovinger, A. J. *Polymer* **1996**, *37*, 4979–4992.
(3) Alamo, R. G.; Brown, G. M.; Mandelkern, L.; Lehtinen, A.; Paukkeri, R. *Polymer* **1999**, *40*, 3933–3944.
(4) Meille, S. V.; Ferro, D. R.; Bruckner, S.; Lovinger, A. J.; Padden, F. J. *Macromolecules* **1994**, *27*, 2615–2622.
(5) Meille, S. V.; Bruckner, S.; Porzio, W. *Macromolecules* **1990**, *23*, 4114–4121.
(6) Mezghani, K.; Phillips, P. J. *Polymer* **1998**, *39*, 3735–3744.
(7) Foresta, T.; Piccarolo, S.; Goldbeck-Wood, G. *Polymer* **2001**, *42*, 1167–1176.
(8) Leugering, H. J.; Kirsch, G. *Angew. Makromol. Chem.* **1973**, *33*, 17–23.
(9) Varga, J.; Karger-Kocsis, J. *J. Polym. Sci., Part B: Polym. Phys.* **1996**, *34*, 657–670.
(10) Somani, R. H.; Hsiao, B. S.; Nogales, A.; Fruitwala, H.; Srinivas, S.; Tsou, A. H. *Macromolecules* **2001**, *34*, 5902–5909.
(11) Huo, H.; Jiang, S. C.; An, L. J.; Feng, J. C. *Macromolecules* **2004**, *37*, 2478–2483.
(12) Fujiwara, Y. *Colloid Polym. Sci.* **1975**, *253*, 273–282.
(13) Varga, J. *J. Macromol. Sci., Phys.* **2002**, *B41*, 1121–1171.
(14) Leugering, H. J. *Makromol. Chem.* **1967**, *109*, 204–216.
(15) Shi, G.; Zhang, X.; Qiu, Z. *Makromol. Chem.* **1992**, *193*, 583–591.
(16) Varga, J.; Mudra, I.; Ehrenstein, G. W. *J. Appl. Polym. Sci.* **1999**, *74*, 2357–2368.
(17) Ikeda, N.; Kobayashi, T.; Killough, L. *Polypropylene '96*; World Congress: Zurich, Switzerland, Sept 18−20, 1996.
(18) Mathieu, C.; Thierry, A.; Wittmann, J. C.; Lotz, B. *J. Polym. Sci., Part B: Polym. Phys.* **2002**, *40*, 2504–2515.
(19) Menyhárd, A.; Varga, J.; Molnár, G. *J. Therm. Anal. Calorim.* **2006**, *83*, 625–630.
(20) Krache, R.; Benavente, R.; López-Majada, J. M.; Pereña, J. M.; Cerrada, M. L.; Pérez, E. *Macromolecules* **2007**, *40*, 6871–6878.
(21) Zhao, S. C.; Cai, Z.; Xin, Z. *Polymer* **2008**, *49*, 2745–2754.
(22) Dong, M.; Su, Z. Q.; Guo, Z. X.; Yu, J. *J. Polym. Sci., Part B: Polym. Phys.* **2008**, *46*, 1183–1192.
(23) Dong, M.; Guo, Z. X.; Yu, J.; Su, Z. Q. *J. Polym. Sci., Part B: Polym. Phys.* **2008**, *46*, 1725–11733.

(24) Bai, H. W.; Wang, Y.; Liu, L.; Zhang, J. H.; Han, L. *J. Polym. Sci., Part B: Polym. Phys.* **2008**, *46*, 1853–1867.
(25) Yi, Q. F.; Wen, X. J.; Dong, J. Y.; Han, C. C. *Polymer* **2008**, *49*, 5053–5063.
(26) Varga, J.; Ehrenstein, G. W. *Colloid Polym. Sci.* **1997**, *275*, 511–519.
(27) Trifonova, D.; Varga, J.; Ehrenstein, G. W.; Vancso, G. J. *J. Polym. Sci., Polym. Phys.* **2000**, *38*, 672–681.
(28) Karger-Kocsis, J.; Varga, J. *J. Appl. Polym. Sci.* **1996**, *62*, 291–300.
(29) Coulon, G.; Castelein, G.; G'Sell, C. *Polymer* **1999**, *40*, 95–110.
(30) Aboulfaraj, M.; G'Sell, C.; Ulrich, B.; Dahoun, A. *Polymer* **1995**, *36*, 731–742.
(31) Tordjeman, Ph.; Robert, C.; Marin, G.; Gerard, P. *Eur. Phys. J. E* **2001**, *4*, 459–465.
(32) Henning, S.; Adhikari, R.; Michler, G. H.; Baltá Calleja, F. J.; Karger-Kocsis, J. *Macromol. Symp.* **2004**, *214*, 157–171.
(33) Chen, H. B.; Karger-Kocsis, J.; Wu, J. S.; Varga, J. *Polymer* **2002**, *43*, 6505–6514.
(34) Karger-Kocsis, J.; Varga, J.; Ehrenstein, G. W. *J. Appl. Polym. Sci.* **1997**, *64*, 2057–2066.
(35) Karger-Kocsis, J. *Polym. Eng. Sci.* **1996**, *36*, 203–210.
(36) Kotek, J.; Raab, M.; Baldrian, J.; Grellmann, W. *J. Appl. Polym. Sci.* **2002**, *85*, 1174–1184.
(37) Kotek, J.; Kelnar, I.; Baldrian, J.; Raab, M. *Eur. Polym. J.* **2004**, *40*, 679–684.
(38) Ščudla, J.; Raab, M.; Eichhorn, K.-J.; Strachota, A. *Polymer* **2003**, *44*, 4655–4664.
(39) Varga, J.; Menyhárd, A. *Macromolecules* **2007**, *40*, 2422–2431.
(40) Varga, J.; Tóth, F. *Makromol. Chem., Makromol. Symp.* **1986**, *5*, 213–223.
(41) Trifonova, D.; Varga, J.; Vancso, G. J. *Polym. Bull.* **1998**, *41*, 341–348.
(42) Varga, J. *J. Therm. Anal.* **1989**, *35*, 1891–1912.
(43) Davies, R. J.; Zafeiropoulos, N. E.; Schneider, K.; Roth, S. V.; Burghammer, M.; Riekel, C.; Kotek, J. C.; Stamm, M. *Colloid Polym. Sci.* **2004**, *282*, 854–866.
(44) Ferrer-Balas, D.; Maspoch, M. L.; Martinez, A. B.; Santana, O. O. *Polymer* **2001**, *42*, 1697–1705.
(45) Frontini, P. M.; Fave, A. *J. Mater. Sci.* **1995**, *30*, 2446–2454.
(46) Ito, J.-I.; Mitani, K.; Mizutani, Y. *J. Appl. Polym. Sci.* **1992**, *46*, 1221–1233.
(47) Olley, R. H.; Bassett, D. C. *Polymer* **1982**, *23*, 1707–1710.
(48) Li, J. X.; Cheung, W. L.; Jia, D. *Polymer* **1999**, *40*, 1219–1222.
(49) Bai, H. W.; Wang, Y.; Song, B.; Li, Y. L.; Liu, L. *Polym. Eng. Sci.* **2008**, *48*, 1532–1541.
(50) Yalcin, B.; Cakmak, M. *Polymer* **2004**, *45*, 2691–2710.
(51) Turner Jones, A.; Aizlewood, J. M.; Beckett, D. R. *Makromol. Chem.* **1964**, *75*, 134–158.
(52) Fiebig, J.; Gahleitner, M.; Paulik, C.; Wolfschwenger, J. *Polym. Test.* **1999**, *18*, 257–266.
(53) Li, Q. G.; Xie, B. H.; Yang, W.; Li, Z. M.; Zhang, W. Q.; Yang, M. B. *J. Appl. Polym. Sci.* **2007**, *103*, 3438–3446.
(54) Bai, H. W.; Wang, Y.; Song, B.; Li, Y. L.; Liu, L. *Polym. Eng. Sci.* **2008**, *48*, 1532–1541.
(55) Ferrer-Balas, D.; Maspoch, M. L.; Martinez, A. B.; Santana, O. O. *Polymer* **2001**, *42*, 1697–1705.
(56) Zia, Q.; Mileva, D.; Androsch, R. *Macromolecules* **2008**, *41*, 8095–8102.
(57) Hedesiu, C.; Demco, D. E.; Kleppinger, R.; Vanden Poel, G.; Gijsbers, W.; Blumich, B.; Remerie, K.; Litvinov, V. M. *Macromolecules* **2007**, *40*, 3977–3989.
(58) Hedesiu, C.; Demco, D. E.; Kleppinger, R.; Vanden Poel, G.; Remerie, K.; Litvinov, V. M.; Blumich, B.; Steenbakkers, R. *Macromol. Mater. Eng.* **2008**, *293*, 847–857.
(59) Maiti, P.; Hikosaka, M.; Yamada, K.; Toda, A.; Gu, F. *Macromolecules* **2000**, *33*, 9069–9075.
(60) Alamo, R. G.; Brown, G. M.; Mandelkern, L.; Lehtinen, A.; Paukkeri, R. *Polymer* **1999**, *40*, 3933–3944.
(61) Xu, W.; Martin, D. C.; Arruda, E. M. *Polymer* **2005**, *46*, 455–470.
(62) Menyhárd, A.; Varga, J. *Eur. Polym. J.* **2006**, *42*, 3257–3268.
(63) Norton, D. R.; Keller, A. *Polymer* **1985**, *26*, 704–716.
(64) Tanniru, M.; Yuan, Q.; Misra, R. D. K. *Polymer* **2006**, *47*, 2133–2146.
(65) Yuan, Q.; Misra, R. D. K. *Polymer* **2006**, *47*, 4421–4433.
(66) Deshmane, C.; Yuan, Q.; Misra, R. D. K. *Mater. Sci. Eng., A* **2007**, *452*−*453*, 592–601.
(67) Ravi, S.; Takahashi, K. *Polym. Eng. Sci.* **2002**, *42*, 2146–2155.
(68) Kim, G.-M.; Michler, G. H.; Gahleitner, M.; Fiebig, J. *J. Appl. Polym. Sci.* **1996**, *60*, 1391–1403.
(69) Glatter, O.; Kratky, O. *Small-Angle X-ray Scattering*; Academic Press: London, UK, 1982.
(70) Pawlak, A.; Galeski, A. *Macromolecules* **2008**, *41*, 2839–2851.
(71) Boyd, R. H. *Polymer* **1985**, *26*, 323–347.
(72) Read, B. E. *Polymer* **1989**, *30*, 1439–1445.
(73) Alberola, N.; Fugier, M.; Petit, D.; Fillon, B. *J. Mater. Sci.* **1995**, *30*, 1187–1195.
(74) Tajvidi, M.; Falk, R. H.; Hermanson, J. C. *J. Appl. Polym. Sci.* **2006**, *101*, 4341–4349.
(75) Grein, C.; Bernreitner, K.; Gahleitner, M. *J. Appl. Polym. Sci.* **2004**, *93*, 1854–1867.
(76) Jafari, S. H.; Gupta, A. K. *J. Appl. Polym. Sci.* **2000**, *78*, 962–971.
(77) Karger-Kocsis, J.; Kuleznev, V. N. *Polymer* **1982**, *23*, 699–705.
(78) Mccready, M. J.; Schultz, J. M. *J. Polym. Sci., Polym. Phys Ed.* **1979**, *17*, 725–740.